



Title	Transient Stability Enhancement with High Shares of Grid-Following Converters in a 100% Converter Grid
Authors(s)	Zhao, Xianxian, Flynn, Damian
Publication date	2020-10-28
Publication information	Zhao, Xianxian, and Damian Flynn. "Transient Stability Enhancement with High Shares of Grid-Following Converters in a 100% Converter Grid." IEEE, October 28, 2020. https://doi.org/10.1109/isgt-europe47291.2020.9248794 .
Conference details	The 2020 IEEE PES Innovative Smart Grid Technologies Europe (ISGT-Europe), Delft, The Netherlands, 26-28 October 2020
Publisher	IEEE
Item record/more information	http://hdl.handle.net/10197/13085
Publisher's statement	© 2020 IEEE. Personal use of this material is permitted. Permission from IEEE must be obtained for all other uses, in any current or future media, including reprinting/republishing this material for advertising or promotional purposes, creating new collective works, for resale or redistribution to servers or lists, or reuse of any copyrighted component of this work in other works.
Publisher's version (DOI)	10.1109/isgt-europe47291.2020.9248794

Downloaded 2026-05-01 23:43:28

The UCD community has made this article openly available. Please share how this access benefits you. Your story matters! (@ucd_oa)



© Some rights reserved. For more information

Transient Stability Enhancement with High Shares of Grid-Following Converters in a 100% Converter Grid

Xianxian Zhao and Damian Flynn
School of Electrical and Electronic Engineering
University College Dublin
Dublin, Republic of Ireland
xianxian.zhao@ucd.ie, damian.flynn@ucd.ie

Abstract—With increasing shares of power electronics-based generation in power grids, grid-following converters may become unstable during faults, resulting from a loss of phase-locked loop (PLL) synchronism. Even when current grid code low voltage ride through (LVRT) requirements are met, PLLs may still become unstable under high shares of grid-following converters, due to much reduced reactive current support from (online) synchronous generators or grid-forming converters. Consequently, a readily implementable transient stability enhancement approach is developed for grid-following converters using a reactive current priority current limiting strategy for faults on a transmission network. The proportional gain for the reactive current injection is determined by formulating an optimization-based transient stability problem, which ensures a valid PLL equilibrium point, maximizes active power output, fully exploits converter current capacity, and, at least, satisfies existing grid code LVRT requirements. An additional PLL frequency-feedback PI term is used to enhance PLL dynamic stability, in recognition of parameter estimation errors and imperfect control. A case study (100% converter-based grid) verifies that the proposed solution enables grid robustness against faults and the permissible share of grid-following converters to be increased (especially in weak grids).

Keywords—Grid-forming converter, grid-following converter, phase-locked loop, transient stability, low voltage ride through

I. INTRODUCTION

Electric power systems are undergoing a period of unprecedented change, with conventional generation, based around synchronous machines, being replaced by renewable energy sources that are connected to the system via power converters [1]. However, while power converters can provide a much faster and more flexible response, when compared against synchronous generators (SGs), their full impact on power system operation, stability and control remains to be fully investigated. At present, power converters are controlled as current sources by injecting a given active and reactive power to the grid. To realize this injection, a phase-locked loop (PLL) synchronizes the converter with the grid frequency, based on measurement of the converter terminal voltage. Consequently, such converters are termed as 'grid-following' or 'grid-feeding'.

Under this control principle, the permissible share of converters can be limited for two main reasons. Firstly, the converter share cannot reach 100% since there wouldn't then be a 'frequency source' to follow [2]. Secondly, at higher converter shares, with fewer online voltage and frequency regulation units, the AC voltage can vary more dramatically [3], making the synchronization process more challenging [4]. It, therefore, becomes necessary to identify those factors which impact the stability of PLLs, and to modify these controls to ensure that the system can operate successfully under more challenging conditions. Moving forward with higher converter shares, in the near future, some power

converters, known as 'grid-forming', must behave as voltage sources, being able to regulate the voltage and frequency. In addition, the control of existing and/or future grid-following converters should be modified to enhance system robustness and reduce regulation requirements.

Small-signal and large-signal models, and stability analysis of grid-following converters are examined in [5] and [6]-[10], respectively. It is shown that the PLL is the critical component for the stability of a grid-following converter under both small and large disturbances. Although several methods have been proposed for transient stability enhancement [6]-[10], there is still much which could be improved. For example, in [6][7], a low bandwidth PLL, or PLL 'freezing', is suggested during faults. However, it can be difficult to judge when to switch between the normal and 'frozen' PLLs. In addition, using a low bandwidth PLL leads to poor damping, especially at higher short-circuit ratios, and a slow dynamic response to setpoint or network topology changes [5]. Adaptive PLL gain tuning [8] can enhance stability, but the existence of a PLL equilibrium point cannot be ensured. In [9], the ratio of active and reactive current references is designed to match the equalized grid impedance R/X ratio. However, the active current reference reduces to a very small value for transmission networks, when the R/X ratio is small. In practice, the active current reference can be much larger. In [10], the PLL frequency negative feedback-based method is robust to different operating conditions, but a current scaling limiting strategy was used, and converter current capacity was not fully exploited.

This paper focuses on enhancing the transient stability of power systems with a high share of grid-forming converters, and contributes mainly in the following two aspects:

- A simple, but practical, transient stability approach for grid-following converters in transmission networks is proposed. By formulating transient stability concerns as an optimization problem, a PLL equilibrium point is obtained which maximizes active power output, fully exploits converter current capacity, and, at least, satisfies grid code LVRT requirements. A further PLL frequency negative feedback PI term ensures PLL dynamic stability, considering parameter estimation errors during optimization formulation and imperfect current control. With reactive current prioritized, PI parameters are less sensitive to changes in system conditions.
- A practical simulation scenario is set up and simulated: the New England 39-bus test system is modified by replacing all synchronous units with grid-following and grid-forming converters; different grid-following shares are studied with different controls under fault conditions, in order to confirm that the grid-following share can be much increased, while the grid remains transiently stable with little oscillations under symmetrical bolted faults.

The remainder of the paper is organized as follows. Section II introduces the control strategy, and the PLL model of the grid-following converters. Section III presents the transient stability solution and controller parameter tuning. Section IV presents simulation results, while Section V summarizes the conclusions.

II. GRID-FOLLOWING CONVERTER

A grid-following converter connected to an equivalent AC grid is shown in Fig. 1, where R_f and L_f are the resistance and inductance of the converter output filter, and R_g and L_g are the equivalent grid resistance and inductance. The converter uses a PLL (in the standard synchronous reference frame) to passively follow the terminal voltage phase to achieve synchronization with the AC grid.

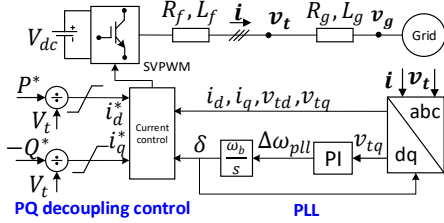


Fig. 1. Grid-following converter connected to an equivalent AC grid.

Once synchronized, the q-axis and d-axis terminal voltages in the obtained synchronous dq-frame become 0 and V_t (amplitude of converter terminal voltage \mathbf{v}_t). Hence, the converter active and reactive output power are decoupled and can be controlled independently by the d-axis (i_d) and q-axis (i_q) currents. Therefore, during normal operation the grid-following converter can output active and reactive power setpoints of P^* and Q^* using the current references below:

$$i_d^* = \frac{P^*}{V_t} \quad (1) \quad i_q^* = -\frac{Q^*}{V_t} \quad (2)$$

Since active current is prioritized under normal operation, $|i_d^*| \leq I_{max}$ and $|i_q^*| \leq \sqrt{I_{max}^2 - i_d^{*2}}$, where I_{max} represents the maximum allowable current of the converter. Now considering the PLL model and prerequisites for its stability, from Fig. 1 it follows that

$$\mathbf{v}_t^s = \mathbf{v}_g^s + R_g \mathbf{i}^s + L_g \frac{d\mathbf{i}^s}{d(\omega_b t)} \quad (3)$$

where ω_b is the base angle frequency, and superscript s indicates the voltage and current vectors in the stationary reference frame. Since $\mathbf{v}_t = \mathbf{v}_t^s e^{-j\theta_{pll}}$ and $\mathbf{i} = \mathbf{i}^s e^{-j\theta_{pll}}$, with $\delta = \theta_{pll} - \theta_g$, by assuming that the converter output current equals the current reference, it is seen that

$$v_{td} = V_g \cos \delta + R_g i_d^* - (\omega_0 + \Delta\omega_{pll}) L_g i_q^* \quad (4)$$

$$v_{tq} = -V_g \sin \delta + R_g i_q^* + (\omega_0 + \Delta\omega_{pll}) L_g i_d^* \quad (5)$$

where $\omega_0 = 1.0$ is the nominal angular frequency. The PI and integrator operators before and after $\Delta\omega_{pll}$ are given by

$$\hat{\delta} = \omega_b \Delta\omega_{pll}, \quad (6)$$

$$\Delta\omega_{pll} = K_p v_{tq} + K_i \int v_{tq}. \quad (7)$$

The PLL model can be suitably expressed in the form of $f_1 \delta + f_2 \dot{\delta} + f_3 \sin \delta = f_4$ by combining (1), (2) and (4)-(7), together with the specific current limiting strategy, where f_i , $i = 1 \dots 4$, are functions of V_g , R_g , L_g , and/or P^* and Q^* . If the PLL is stable, then $v_{tq} = 0$. Thus, based on (5), the necessary condition for PLL stability (condition of existence of equilibrium point [6], or within the transfer limit of the transmission line [10]) can be obtained as

$$|L_g i_d^* + R_g i_q^*| \leq V_g. \quad (8)$$

It should be noted that condition (8) doesn't provide the final representation, since i_d^* and i_q^* are given by (1) and (2) under normal conditions, while, during faults, based on the LVRT grid code of [11], they are given by

$$i_q^* = -\min(1, 2(0.9 - V_t)), \quad V_t < 0.9, \quad (9)$$

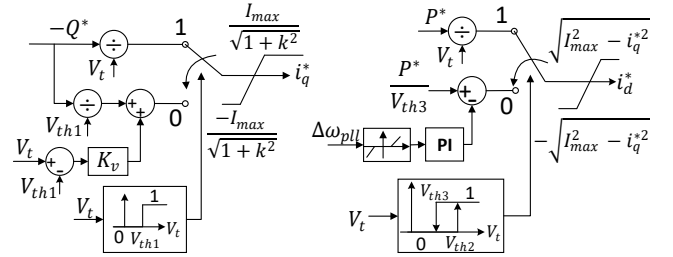
$$i_d^* = \min\left(\sqrt{I_{max}^2 - i_q^{*2}}, \frac{P^*}{V_t}\right), \quad V_t < 0.9. \quad (10)$$

The current reference design in (9) and (10) during faults may not satisfy (8), especially for a weak grid (large L_g) or a system with a high share of grid-following converters, where the equalized grid voltage, V_g , may be low during faults due to synchronous generators being replaced by converters, with much smaller reactive support capability. From (8), it can be seen that by actively reducing i_d^* and i_q^* (i_q^* should be negative) during faults, V_g can be increased and the value of the left hand of (8) can be decreased. In this way, the PLL (and grid-following converter) remains stable.

III. PROPOSED TRANSIENT STABILITY SOLUTION

A. Proposed Transient Stability Solution

A simple practical transient stability solution, shown in Fig. 2, is now proposed which (1) ensures the existence of a stable PLL operating point, (2) maximizes active power injection, (3) fully exploits converter current capacity, and, (4) at least, satisfies grid code LVRT requirements [11].



(a) Reactive current reference design (b) Active current reference design
Fig. 2. Control diagram of proposed transient stability solution.

To realize the above objectives, for transmission network with small R_g/L_g and grid-following with fast PLLs, reactive current is proposed to be prioritized during faults, and the current references are given as

$$i_q^* = \begin{cases} -\frac{Q^*}{V_t}, & V_t \geq V_{th1} \\ -K_v(V_{th1} - V_t) - \frac{Q^*}{V_{th1}}, & V_t < V_{th1} \end{cases} \quad (11)$$

$$i_d^* = \begin{cases} \frac{P^*}{V_t}, & V_t \geq V_{th2} \\ \frac{P^*}{V_{th3}} - \left(K_{pf} + \frac{K_{if}}{s}\right) \Delta\omega_{pll}, & V_t < V_{th3} \end{cases} \quad (12)$$

where $\Delta\omega_{pll}$ is $\Delta\omega_{pll} \mp \Delta\omega_{db}$, K_v , K_{pf} and K_{if} are positive constants. V_{th1} , V_{th2} and V_{th3} are switching thresholds of the hysteresis comparators.

For the proposed control, by suitably choosing K_v , i_d^* will be automatically given by $\sqrt{I_{max}^2 - i_q^{*2}}$ since i_q^* is prioritized during the fault with the constraint of the existence of a PLL equilibrium point. Thus, the converter current capacity is fully used. PLL frequency based PI negative feedback control is employed in order to enhance PLL stability considering system dynamic uncertainties, only being activated when $\Delta\omega_{pll}$ is outside the deadband. Both

proportional and integral terms are used because the former is useful during the initial phase of a fault before the integral term catches up, while the integral term becomes dominant when the PLL is in steady-state, i.e. $\Delta\omega_{pll}$ is close to zero. In order to smoothly switch i_q^* between normal and fault modes in (11), Q^*/V_{th1} is used when $V_t < V_{th1}$. Tuning of K_v , k , K_{pf} and K_{if} will be presented in Section III.B.

It should be noted that: 1) only symmetrical faults are considered here, although the proposed method is applicable to non-symmetrical faults. Under unbalanced conditions, positive- and negative-sequence current components should be controlled separately in the synchronous reference frame with simple PI controllers in order to limit converter currents to a pre-defined threshold, as shown in [12]. 2) for distribution networks, scaling down current limiting strategy,

$$i_d^* = \frac{i_d'^*}{\sqrt{i_d'^*{}^2 + i_q'^*{}^2}}, \quad i_q^* = \frac{i_q'^*}{\sqrt{i_d'^*{}^2 + i_q'^*{}^2}} \quad \text{when } \sqrt{i_d'^*{}^2 + i_q'^*{}^2} \geq I_{max}$$

where $i_d'^*$ and $i_q'^*$ are from (1) and (2), is preferred since the ratio R_g/L_g is large. For transmission networks, reactive current prioritized strategy is used, compared to other current limiting strategies, because this helps to make PLL stability much less sensitive to the PI parameters K_{pf} and K_{if} .

B. Parameter Tuning

1) Determination of K_v , voltage gain

In order to realize the objectives of the proposed transient stability solution, based on objectives 1, 2 and 4 (Section III.A), the optimization problem (13) is formulated as:

$$\max P = V_t i_d^* \quad (13a)$$

$$\text{subject to } V_g \cos\delta + R_g i_d^* - L_g i_q^* = V_t \quad (13b)$$

$$V_g \sin\delta - R_g i_q^* - L_g i_d^* = 0 \quad (13c)$$

$$i_q^* = K_v (V_t - V_{th1}) - \frac{Q^*}{V_{th1}} \quad (13d)$$

$$i_d^{*2} + i_q^{*2} \leq I_{max}^2 \quad (13e)$$

$$-1 \leq P \leq 1 \quad (13f)$$

where V_t , i_d^* , i_q^* and δ are decision variables, and V_g and K_v are given variables. Constraint (13a) maximizes the active power output, (13b) and (13c) ensure the existence of a PLL equilibrium point, (13d) ensures that grid code LVRT requirements are, at least, satisfied, (13e) respects the current limit, while (13f) limits the active power output to 1 pu.

A suitable value for K_v can be found if it ensures problem feasibility under the specified range of V_g , [0.001, 1] pu, in this paper. Given that $I_{max} = 1.2$ pu [11], $R_g = 0.05$ pu, $L_g = 0.5$ pu, $Q^* = 0$ pu, and $V_{th1} = 0.9$ pu, increasing K_v gradually from 2 ($K_v = 2$ meets the minimum grid code LVRT requirement in [11]), the largest K_v ensuring problem feasibility over the whole range of V_g is 4.1.

Fig. 3 presents the converter active power output, current references, and terminal voltage for 4 different K_v values. Fig. 3(a) shows that with higher K_v , the active power is increased, mainly due to reactive current support, as seen in Fig. 3(b) and Fig. 3(c), where i_d^* is almost the same, but $|i_q^*|$ and V_t increase with higher K_v . Fig. 3(d) shows converter current capacity is only fully utilized beyond $K_v = 4.1$ (note that when V_g is high, there remains unused current capacity under all K_v values, since active power output, P , is limited to 1 pu). Fig. 3(a) shows that with $K_v = 6.1$, further increase

of active power is minimal, and Fig. 3(a)-(c) show that the active current loses its regulation capability when V_t is high. Although large K_v improves PLL stability by fully utilizing converter capacity, it can reduce damping and introduce converter oscillations (cf. Section IV). According to the above analysis, K_v is chosen here as 4.1, so that the active current is automatically assigned to 'unused' current capacity, i.e. $i_d^* = \sqrt{I_{max}^2 - i_q^{*2}}$, and thus the third objective (Section III.A) of using the full current capacity is satisfied, assuming the existence of a PLL equilibrium point across the entire range [0.001, 1] pu for V_g .

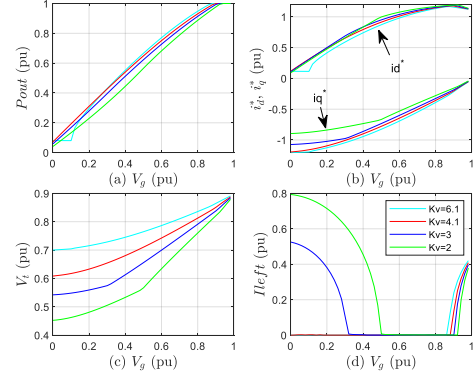


Fig. 3. Results of optimization problem (13) with different K_v .

2) Determination of k

It can be seen from (11) that $|i_q^*|$ is limited within $\frac{I_{max}}{\sqrt{1+k^2}}$ instead of I_{max} . Otherwise the PLL will output a decreasing frequency under low V_t , as seen in [10]. k can be determined by i_q^* at lowest V from the above optimization solution. In fact $k = R_g/L_g$ (the condition that the PLL is globally stable according to the proof in [9]).

Normally, k is selected in the range 0.05~0.15. If the estimated k is larger than the real value k_0 , an additional PLL output frequency PI term (12) can stabilize the PLL. If, instead, k is smaller than k_0 , the PLL will output a decreasing frequency when V_t is very low, i.e. when $V_t < \frac{Gk_0L_g}{\sqrt{1+k^2}} I_{max}$, and $k = (G+1)k_0$ (G represents the estimation error). Suppose $L_g = 1$ pu, $G = 20\%$, $k_0 = 0.1$, and $I_{max} = 1.2$ pu, the PLL outputs a decreasing frequency only when $V_t < 0.024$ pu. However, if $|i_q^*|$ is limited within I_{max} , this occurs when $V_t < k_0 L_g I_{max} = 0.12$ pu. It can be noted that frequency decreasing instability, when the voltage is very low, is not of great concern, but frequency increasing instability is more serious and may happen more frequently. It is also noted that $|i_q^*|$ is not limited to 1 pu, as suggested by the grid code [11], considering that the (transient) overcurrent capacity is usually of the order of 1.2 pu [11].

3) Determination of K_{pf} and K_{if} , PI gains

With k and K_v suitably tuned, a stable operating point can be achieved, based on an estimated network impedance, perfect current tracking and no measurement delays. An additional PI term can be used to enhance PLL stability, to cope with variations in the above, and being activated only when $\Delta\omega_{pll}$ lies outside the deadband. Since i_q^* is prioritized, a sufficiently large K_{pf} and K_{if} can ensure $\Delta\omega_{pll}$ stability.

IV. CASE STUDIES

The New England ten-machine 39-bus system [13] is used to validate the performance of the proposed transient

stability solution. Each synchronous generator is replaced by in parallel grid-following and grid-forming converters with droop control, with a rated capacity of ηS_0 and $(1 - \eta)S_0$, respectively, where S_0 is the same as the original generator rated capacity, and $0 < \eta < 1$. The parameters of the output filter, voltage control and current control for a grid-forming converter follow those in [2][14]. The grid-following model and control parameters follow those in [13], while other parameters, from Fig. 2, are $V_{th1} = V_{th2} = V_{t0} - 0.05$ pu, $V_{th3} = V_{t0} - 0.1$ pu, where V_{t0} is the pre-fault value of V_t , $k = 0.1$, and $\Delta\omega_{db} = 0.001$ pu. I_{max} for both converter types is set at 1.2 pu [11]. A threshold virtual impedance current limitation method [4] is used for the grid-forming converters. A constant DC voltage is assumed for the converters, such that the effect of prime movers is not considered, and system stability issues arise only from the converter controls. The active and reactive power setpoints for the grid-following and grid-forming converters remain the same as the original generators. All loads are modeled as constant impedances, and all quantities are expressed in per-unit except ω_b , base frequency of 314 rad/s. Simulations are performed in Dymola environment using the Modelica language, which readily enables transparency of system component models and control algorithms.

It should be noted that: (i) 100% converter-based generation is chosen here, since it represents the worst case for grid-following PLL stability, considering the much smaller overload capability of converters compared to synchronous units, (ii) only threshold virtual impedance is applied here for grid-forming converters to reduce the converter current, which cannot be strictly limited to a pre-fault value. This is beneficial for transient stability, since the converters can give larger support when necessary, and the downsides of a “hard current limit” for grid-forming converters are avoided, (iii) the grid-forming converter control parameters, based on the tuning algorithm of [4], guarantee stable behavior for different operating conditions. The PLL PI gains ensure fast voltage angle tracking capability and strong damping under normal operation and network disturbances, e.g. line disconnection, which is seen by the simulation results of [14]. The current control PI gains of the grid-following converters ensure sufficiently fast current tracking. Moreover, [14] shows that there are minimal interactions between the grid-forming and grid-following converters under small and large disturbances.

Case 1: 3 control methods for grid following converters are simulated: *no action* (constant PQ control with active current prioritized), *grid-code* (control of (1) and (11) with i_q^* limit modified to 1.2 pu) and *proposed* (solution in (11)-(12)). Here, in Fig. 2, $K_v = 4.1$, $K_{pf} = 0$ and $K_{if} = 5$. A symmetrical 3-phase bolted fault is applied at bus 2 at 2 s and cleared at 2.25 s for each method. To identify the max grid-following share, the η ratio for *no action*, *grid code* and *proposed* are 70%, 80% and 95%, respectively. The η values shown for the different control strategies roughly represent an upper grid-following boundary, since for lower η the system is stable, with small oscillations during the fault conditions. It follows that the proposed control enables the grid-following share to be increased in a strong grid.

Fig. 4(a)-(f) shows the results of the different control strategies (and grid-following share) for the grid-following converter at bus 37. From Fig. 4(a), it is seen that the voltage at bus 37 experiences large oscillations under *no*

action and *grid code* options during the fault, but only minor oscillations under *proposed*. Fig. 4(b) shows the PLL frequency of the grid-following converter at bus 37 (close to the fault location), while during the fault the PLL is only stable under the proposed control, and the PLL loses stability under both other methods. Fig. 4(c)-(d) show the active and reactive current references under all methods. With *no action*, i_d^* is increased to 1.2 pu (maximum) so i_q^* is limited to 0. Under *grid code*, i_d^* is limited by i_q^* when i_q^* reaches the lower limit of -1.2 pu. Under *proposed*, i_d^* is also increased and has the same capability as *grid code*, but the magnitude of i_q^* is smaller. Even with a reduced i_q^* magnitude, the PLL is stable during the fault (red line in Fig. 4(b)), since the terminal voltage V_t under *proposed* is much higher than the other two methods (as seen from Fig. 4(a)), resulting from the stronger reactive power support ($K_v = 4.1$) from other grid-following converters under the proposed control. With a higher V_t , active and reactive power output under the proposed method is the largest across the three methods, as seen from Fig. 4(e)(f). It is noted that under *grid-code* control, with $K_v = 4.1$, at $\eta = 80\%$ the PLL at bus 37 is stable but with large oscillations during faults, similar to the *No-PLL-feedback+larger- K_v* control in Case 2. Fig. 4(g)(h) show the current from the grid-forming converters at bus 31 and bus 36. Under *no action* and *grid code* the currents exceed the maximum value of 1.2 pu while under *proposed* the current remains below the limit during the fault, implying that under *proposed*, a lower regulation requirement is needed.

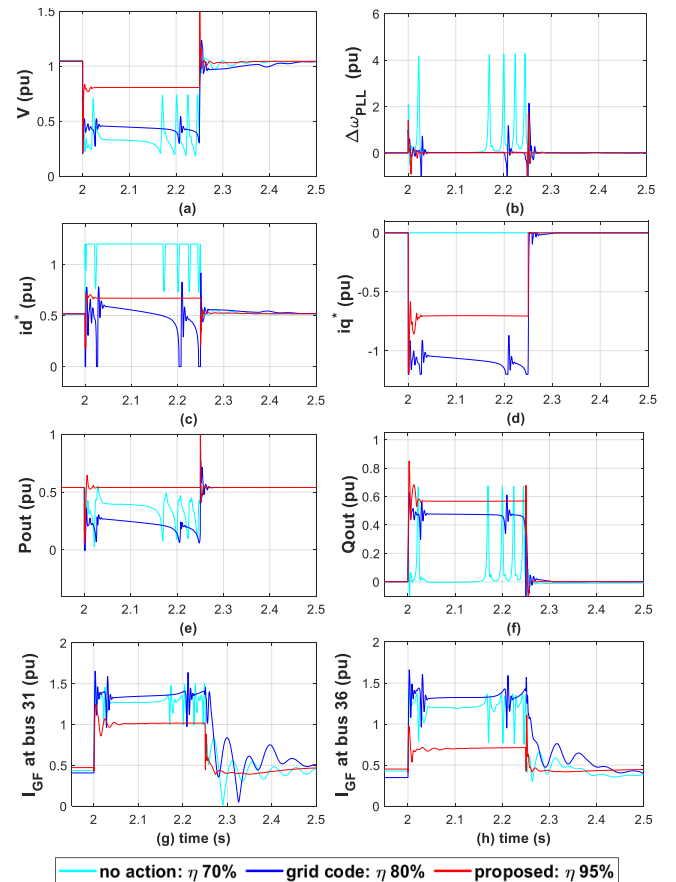


Fig. 4. Impact of different control strategies and grid-following share η for 250 ms 3-phase fault at bus 2.

Case 2: The 39-bus system is made weaker by introducing additional line impedance ($R = 0.02$ pu, $L = 0.08$ pu) for

each generation node connection. To maintain the terminal voltage within normal range, active and reactive power setpoints are also modified. Two sets of simulations are conducted, whereby a symmetrical three-phase bolted fault is applied at bus 16 at 2 s and cleared at 2.25 s. Group A: The above three controls are simulated. Simulation results (not shown, but similar to Case 1) show that the system is stable until the grid following η ratio for *no action* and *grid code* reaches 55% and 75% (with 5% step change), while for *proposed* ($K_v = 4.1$, $K_{pf} = 20$ and $K_{if} = 0$) the system is stable at 95%. Group B: 3 new situations are defined: 1) $\eta = 74\%$, $K_v = 4.1$, $K_{pf} = 0$ and $K_{if} = 0$, termed *No-PLL-feedback*, 2) $\eta = 74\%$, $K_v = 6.1$, $K_{pf} = 0$ and $K_{if} = 0$, termed *No-PLL-feedback+larger- K_v* , and 3) $\eta = 95\%$, $K_v = 4.1$, $K_{pf} = 20$ and $K_{if} = 0$, termed as *PLL feedback*. Results for grid-following converters at bus 32 and 36 are shown in Fig. 5. Note post-fault oscillations, due to limited system damping capability, since grid-forming share is low.

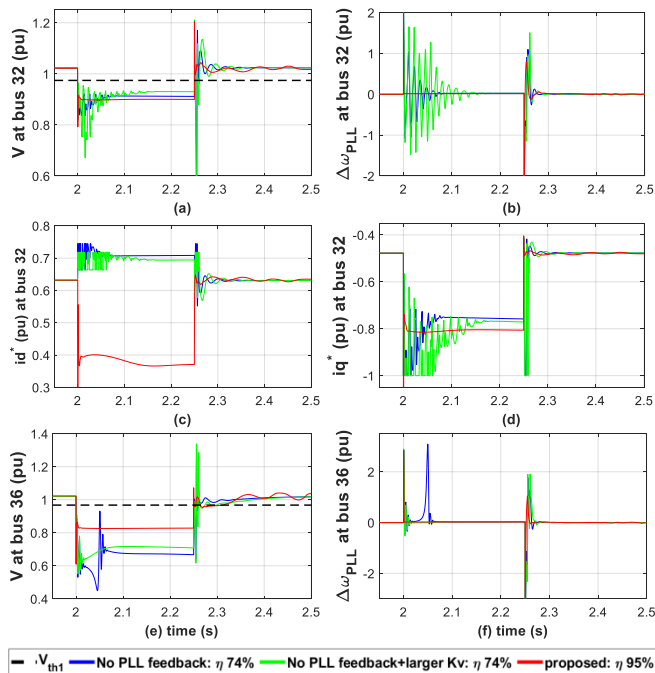


Fig. 5. Impact of PLL feedback term and reactive current gain for 250 ms 3-phase fault at bus 16.

Fig. 5(a)-(b) and (e)-(f) show that under *PLL feedback*, the voltages have reduced oscillations and the PLLs are very stable during faults, even when $\eta = 95\%$, while under *No-PLL-feedback* and *No-PLL-feedback+larger- K_v* , there are $\Delta\omega_{pll}$ oscillations, with stability marginally retained when η hits 74%. It can also be seen that there is little improvement under *No-PLL-feedback+larger- K_v* as compared with *No-PLL-feedback*. Moreover, there are post-fault oscillations when V_t is larger than V_{th1} , arising from the grid-forming converters. Fig. 5(c)-(d) show that under *No-PLL-feedback* and *No-PLL-feedback+larger- K_v* , i_d^* and i_q^* chatter since their designs rely on real-time measurement of V_t . It follows that the PLL feedback term is useful for regulating the active current reference i_d^* and PLL stabilization, especially for weak grids. However, increasing K_v , when it is already large, cannot further enhance system transient stability. Similar results are obtained if K_{if} is changed to 5 in Group B.3, indicating some insensitivity to K_{pf} and K_{if} .

V. CONCLUSION

In order to facilitate higher integration of power converters, a simple practical transient stability solution is proposed for grid-following converters in order to enhance system transient stability and reduce regulation requirements, considering that the overload capability of converters is much less than that of synchronous generators. By optimally selecting the proportional gain for reactive current injection through formulating an optimization problem, a stable PLL operating point is obtained while active power output is maximized during fault conditions. In addition, converter current capacity is fully exploited and grid code LVRT requirements are, at least, satisfied. With reactive current prioritized, an additional PLL frequency feedback PI term is incorporated to maintain PLL stability, considering estimation errors of network parameters and imperfect converter control. Case studies with a high share of grid-following converters in a 100% converter-based system, based on the modified IEEE 39-bus power system, are simulated, to confirm proposed solution effectiveness under symmetrical bolted faults.

ACKNOWLEDGEMENT

Xianxian Zhao is supported by Science Foundation Ireland under Investigator Award SFI/15/IA/3058.

REFERENCES

- [1] F. Milano et al., "Foundations and challenges of low-inertia systems," in *Proc. Power Syst. Comput. Conf.*, Dublin, Ireland, 2018.
- [2] B. Burger, Power Generation in Germany – Assessment of 2016. Fraunhofer Institute for Solar Energy Systems; 017.
- [3] M.J. Korytowski, "Effects of the phase locked loop on the stability of a voltage source converter in a weak grid environment," Ph.D. dissertation, Univ. of Pittsburgh, Pittsburgh, PA, USA, 2014.
- [4] T. Qoria et al., "Local control and simulation tools for large transmission systems," MIGRATE WP3, 2019. Available: <https://www.h2020-migrate.eu/downloads.html>. [Accessed: 26/3/20]
- [5] J.Z. Zhou et al., "Impact of short-circuit ratio and phase-locked-loop parameters on the small-signal behavior of a VSC-HVDC converter," *IEEE Trans. Power Del.*, vol. 29(5), pp. 2287-2296, 2014.
- [6] D. Dong et al., "Analysis of phase-locked loop low-frequency stability in three-phase grid-connected power converters considering impedance interactions," *IEEE Trans. Ind. Electron.*, vol. 62(1), pp. 310-321, 2014.
- [7] M.G. Taul et al., "Robust fault ride through of converter-based generation during severe faults with phase jumps," *IEEE Trans. Ind. Appl.*, vol. 56(1), pp. 570-583, 2020.
- [8] L. Hadjidemetriou et al., "An adaptive tuning mechanism for phase-locked loop algorithms for faster time performance of interconnected renewable energy sources," *IEEE Trans. Ind. Appl.*, vol. 51(2), pp. 1792-1804, 2015.
- [9] S. Ma et al., "Grid-synchronization stability improvement of large scale wind farm during severe grid fault," *IEEE Trans. Power Syst.*, vol. 33(1), pp. 216-226, 2017.
- [10] Ö. Göksu et al., "Instability of wind turbine converters during current injection to low voltage grid faults and PLL frequency based stability solution," *IEEE Trans. Power Syst.*, vol. 29(4), pp. 1683-1691, 2014.
- [11] N. R. Ullah et al., "Voltage and transient stability support by wind farms complying with the E.ON Netz grid code," *IEEE Trans. Power Syst.*, vol. 22(4), pp. 1647-1656, 2007.
- [12] B. Mahamedi et al., "Sequence-based control strategy with current limiting for the fault ride-through of inverter-interfaced distributed generators," *IEEE Trans. Sust. Energy*, vol. 11(1), pp. 165-174, 2018.
- [13] M. Pai, Energy function analysis for power system stability. Springer Science & Business Media, 2012.
- [14] P. Thakurta et al., "Local control and simulation tools for large transmission systems," EU H2020 MIGRATE WP3, 2019. Available: <https://www.h2020-migrate.eu/downloads.html>. [Accessed: 26/3/20]